Life history of the stem tetrapod *Acanthostega* revealed by synchrotron microtomography

Sophie Sanchez[1,2], Paul Tafforeau[2], Jennifer A. Clack[3] & Per E. Ahlberg[1]

The transition from fish to tetrapod was arguably the most radical series of adaptive shifts in vertebrate evolutionary history. Data are accumulating rapidly for most aspects of these events[1–5], but the life histories of the earliest tetrapods remain completely unknown, leaving a major gap in our understanding of these organisms as living animals. Symptomatic of this problem is the unspoken assumption that the largest known Devonian tetrapod fossils represent adult individuals. Here we present the first, to our knowledge, life history data for a Devonian tetrapod, from the *Acanthostega* mass-death deposit of Stensiö Bjerg, East Greenland[6,7]. Using propagation phase-contrast synchrotron microtomography (PPC-SRμCT)[8] to visualize the histology of humeri (upper arm bones) and infer their growth histories, we show that even the largest individuals from this deposit are juveniles. A long early juvenile stage with unossified limb bones, during which individuals grew to almost final size, was followed by a slow-growing late juvenile stage with ossified limbs that lasted for at least six years in some individuals. The late onset of limb ossification suggests that the juveniles were exclusively aquatic, and the predominance of juveniles in the sample suggests segregated distributions of juveniles and adults at least at certain times. The absolute size at which limb ossification began differs greatly between individuals, suggesting the possibility of sexual dimorphism, adaptive strategies or competition-related size variation.

The life cycle of the earliest tetrapods, and its role in the transition from water to land, has long been a matter of speculation. For example, it has been suggested that the earliest tetrapods bred in ephemeral pools, and that the need for the larvae to locomote overland or through extremely shallow water when relocating from these drying ponds to more permanent water bodies provided selective pressure towards the evolution of terrestriality[9]. However, the fossil record of Devonian tetrapods, being dominated by rare and incomplete specimens that frequently come from poorly constrained localities such as scree slopes[10], has until now yielded virtually no life history data.

The only known Devonian tetrapod locality with good potential for revealing life history information is the *Acanthostega* mass-death deposit in the Britta Dal Formation (Upper Devonian, Famennian) on Stensiö Bjerg, East Greenland[10]. This locality, comprising a small *in situ* micaceous silty sandstone body and immediately associated scree[10], has yielded more than 200 skeletal elements. Fourteen skulls, six of them associated with partially articulated skeletons, were complete enough to measure[11], and several more can be identified as individuals; there must have been at least 20 animals represented, although almost certainly more were present. Other vertebrates are represented only by a few isolated bones[7]. The *Acanthostega* individuals in this deposit evidently died together, probably during drought following a sheet-flood event[6]; they thus represent a single time-point sample from a population of this stem tetrapod.

Acanthostega humeri from the mass-death deposit show varying degrees of ossification, representing a possible partial ontogenetic series[11,12]. Using the non-destructive imaging technique PPC-SRμCT[8], performed at beamline ID19 of the European Synchrotron Radiation Facility (ESRF) (see Methods for more details), we have undertaken histological investigations of the four humeri collected from the locality (Natural History Museum of Denmark MGUH 29019, MGUH 29020, NHMD 74756; University Museum of Zoology Cambridge UMZC T.1295)[13] (Fig. 1a and Extended Data Fig. 1), recovering data that illuminate the life history of *Acanthostega*. These are all the humeri of *Acanthostega* known so far. The humerus MGUH 29019 comes from an articulated specimen. The other humeri are isolated bones. The humeri fall into two distinct size classes—large (NHMD 74756, MGUH 29020) and small (MGUH 29019, UMZC T.1295) (Fig. 1a and Extended Data Fig. 1). Consistent with previous observations[12], we found no correlation between size and degree of ossification: specimens NHMD 74756 and UMZC T.1295 are weakly ossified whereas specimens MGUH 29019 and MGUH 29020 are strongly ossified (Fig. 1a and Extended Data Fig. 1).

All humeri exhibit an extensive spongiosa surrounded by a thin compact cortex (Fig. 1a, b). This arrangement resembles that of the humerus of the lobe-finned fish *Eusthenopteron*[14], a less crownward member of the tetrapod stem group[15]. Remnants of calcified cartilage in the metaphyseal region (close to the articular extremities; Extended Data Fig. 2c) show that the spongiosa formed by endochondral ossification as in extant tetrapods[16] and *Eusthenopteron*[14,17]. Tubular structures at the base of the epiphyses (Extended Data Fig. 2a, b) resemble the marrow processes in the growth plate of the humerus of *Eusthenopteron*[14].

The midshaft cortex of all *Acanthostega* humeri contains a dense arrangement of radial vascular canals (Fig. 1c) similar to that of juvenile *Eusthenopteron*[14]. The radial canals connect to a basal mesh of surface-parallel canals (Fig. 1c). In the largest specimen, MGUH 29020, the radial canals vary in diameter between different parts of the scanned area (Fig. 1c), probably reflecting local blood-supply needs. Although the cortex shows evidence of patchy basal erosion in three of the humeri, all appear to retain areas of primary internal cortical surface (Fig. 2). Clusters of large aligned globular cell lacunae between the endosteal bone and the cortex (Fig. 2b, d and Extended Data Fig. 3) can be identified as chondrocyte lacunae by comparison with juvenile *Eusthenopteron*, in which similar lacunae lie between the cortical bone and unresorbed remnants of calcified cartilage[14]. These numerous alignments of chondrocyte lacunae at midshaft (Fig. 2 and Extended Data Fig. 3) mark the perichondral surface of the original cartilaginous humerus. As limb bone growth originates at the midshaft, this implies that the cartilaginous rod was very large relative to the observed final size of the bone, and that cortical bone growth conversely made only a modest contribution to the final size. In other words, the *Acanthostega* individuals grew almost to full observed size before their humeri began to ossify.

[1]Science for Life Laboratory and Uppsala University, Subdepartment of Evolution and Development, Department of Organismal Biology, Evolutionary Biology Centre, Norbyvägen 18A, 752 36 Uppsala, Sweden. [2]European Synchrotron Radiation Facility, 71 Avenue des Martyrs, CS-40220, 38043 Grenoble Cedex, France. [3]University Museum of Zoology, Department of Zoology, University of Cambridge, Downing Street, Cambridge CB2 3EJ, UK.
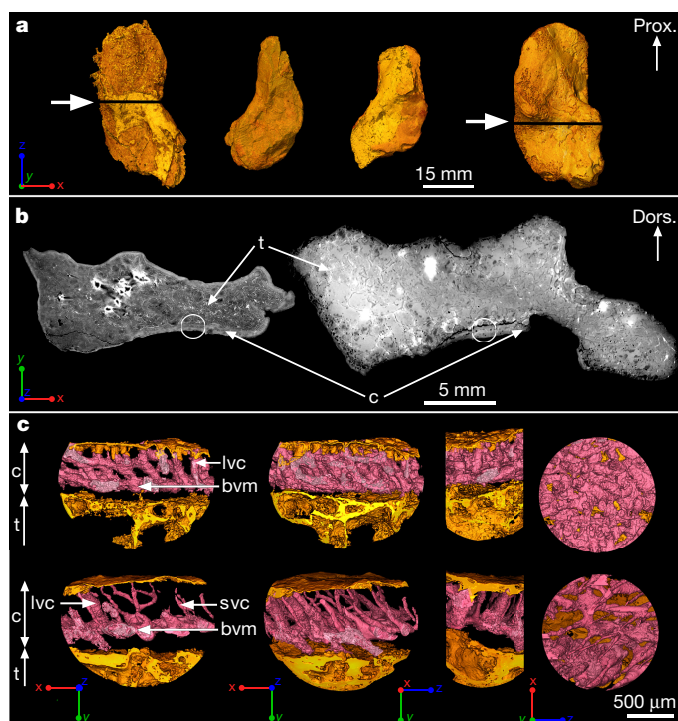
Figure 1 | Midshaft bone microanatomy and histology of *Acanthostega* humeri. a, Three-dimensional models of humeri shown in ventral view, based on synchrotron data. From left to right: NHMD 74756 (voxel size: 14.95 μm), UMZC T.1295 (voxel size: 12.62 μm), MGUH 29019 (voxel size: 12.62 μm) and MGUH 29020 (bottom, voxel size: 20.24 μm). The white arrows indicate the locations of the virtual thin sections in **b. b**, Humeral microanatomy of NHMD 74756 (left) and MGUH 29020 (right) showing an extended trabecular cavity (t) surrounded by a thin layer of compact cortical bone (c). The transverse virtual thin sections are 80 μm thick. The white circles indicate the locations of the high-resolution scans modelled in **c. c**, Three-dimensional models (voxel size: 0.638 μm) of the cortical bone microstructure of NHMD 74756 (top) and MGUH 29020 (bottom) showing a dense oblique mesh of large (lvc) and small (svc) vascular canals (in pink) connected to a horizontal basal vascular mesh (bvm). From left to right: transverse 3D thin section (250 μm thick), complete 3D model in transverse orientation, 3D model in longitudinal orientation and tangential section showing the inner view of the 3D vascular mesh. Dors., dorsal; prox., proximal.

The presence of lines of arrested growth (LAGs) in the cortical bone permits us to infer how many years were occupied by the deposition of this tissue, on the assumption that the deposit between two LAGs represents an annual cycle, as in most extant tetrapods[18,19]. Observations in homologous regions (Extended Data Fig. 4) of the four humeri reveal a maximal number of six LAGs in MGUH 29020 (Fig. 3b, d and Extended Data Fig. 5b, e), four in NHMD 74756 (Fig. 3c, e) and UMZC T.1295 (Extended Data Fig. 5d), and three in MGUH 29019 (Extended Data Fig. 5a, c). All observations were made in areas that were at least partly covered with matrix and thus unlikely to have been affected by external erosion. These LAG patterns are regular and show no tightening (Extended Data Table 1)—that is, no deceleration of the growth rate (Extended Data Fig. 6)—as would be expected at sexual maturity in adult tetrapods[19–21]. This suggests that the four specimens of *Acanthostega* were still juveniles when they died, assuming that their humeri had begun to ossify before the onset of sexual maturity (as they do in all known tetrapods[22–24] and in *Eusthenopteron*[14]; see Supplementary Information). The juvenile stage must therefore have lasted at least six years in *Acanthostega*. Indeed, it probably lasted a good deal longer, because the cartilaginous humerus grew to almost full size before cortical bone deposition, and thus the recording of annual growth increments, even began. *Acanthostega* is not the only member of the tetrapod stem group to show late onset of ossification.

Juvenile *Eusthenopteron* exhibits a large spongiosa and a cortex with no internal resorption, showing that the original cartilaginous rod was approximately two-thirds of adult spongiosa size and presumably formed over several years[14]. How this relates to final adult size in *Acanthostega* is difficult to say, but the slow growth rate of the juvenile *Acanthostega* suggests that final adult size may not have been much greater than the largest individuals recorded from the mass-death deposit.

The complete lack of correlation between size and degree of ossification could reflect some form of individual variation, such as the competition-related size variation observed in certain extant tetrapods[25], adaptive strategies or sexual dimorphism[26]. Under these interpretations, some individuals (represented by MGUH 29019 and UMZC T.1295) began to ossify their humeri—and presumably approach sexual maturity—at a much smaller size than others (represented by MGUH 29020 and NHMD 74756). Unfortunately, the very small sample size does not allow us to determine whether the apparently discrete size classes reflect a real bimodal size distribution, or whether they are simply the outcome of randomly sampling a continuous size variation. However, the observed combination of sizes and ossification states categorically invalidates the construction of an ontogenetic sequence from smallest to largest humerus.

The synchrotron virtual histological data from the humeri shed new light on several aspects of the palaeobiology and life history of *Acanthostega*. It had a prolonged juvenile stage, no less than six years (as shown by the LAGs) but more probably at least a decade, given that it grew almost to full recorded size before the onset of cortical bone ossification. This aligns it with a range of sarcopterygian fishes and tetrapods including *Neoceratodus* (15–20 years[27]), *Eusthenopteron* (adulthood at 11 years[14]), *Discosauriscus* (10 years[20]) and *Andrias* (larval period of 4–5 years and 10 years to adulthood[28]), suggesting that a long juvenile stage could be primitive for tetrapods. The late onset of ossification in *Acanthostega* implies that the early juvenile stage was aquatic, as a cartilaginous humerus would be ill-suited for terrestrial locomotion; this also agrees with the presence of aquatic adaptations such as a large caudal fin and well-developed gill skeleton in *Acanthostega*[1,29], and contradicts the hypothesis of juvenile terrestriality[9] at least for this particular tetrapod.

The fact that all four humeri appear to belong to juvenile individuals suggests that the mass-death assemblage is dominated by, and may in fact consist exclusively of, juveniles. The assemblage does not include a subset of distinctively larger individuals. Specimens MGUH 29019 and MGUH 29020 are the most fully ossified humeri[12] of the assemblage. MGUH 29019, the smallest humerus, is associated with a 12-cm-long skull; MGUH 29020, the largest humerus, is an isolated find from the scree but appears to represent one of the largest individuals in the assemblage (personal observation, J.A.C. and P.E.A.).

The palaeoenvironmental data from the locality provide a context for these observations. It forms part of a large ephemeral fluvial system in an otherwise arid tropical landscape[6], extending northwards for more than 200 km from an unpreserved source water body that must have been large and permanent as it housed large lobe-finned fishes such as *Eusthenodon* and *Holoptychius*[7]. The *Acanthostega* individuals appear to have been flushed out into this fluvial system during a flood event, after which the ensuing drought concentrated them in a shrinking pool and eventually killed them[6]. The almost complete absence of other taxa in the death assemblage suggests that it is not a concentrate of a whole fauna (like the near-contemporary mass-death deposit from Canowindra, Australia[30]) but rather a reflection of schooling behaviour in *Acanthostega*. We can thus tentatively conclude that *Acanthostega* had a long aquatic juvenile stage characterized, at least at certain times, by the formation of schools that included few or no adults.

Whereas the unique palaeoenvironmental and population-related data provided by the *Acanthostega* mass-death deposit are dependent on the context of that particular locality, the type of life history information provided by the humeri is dependent only on the
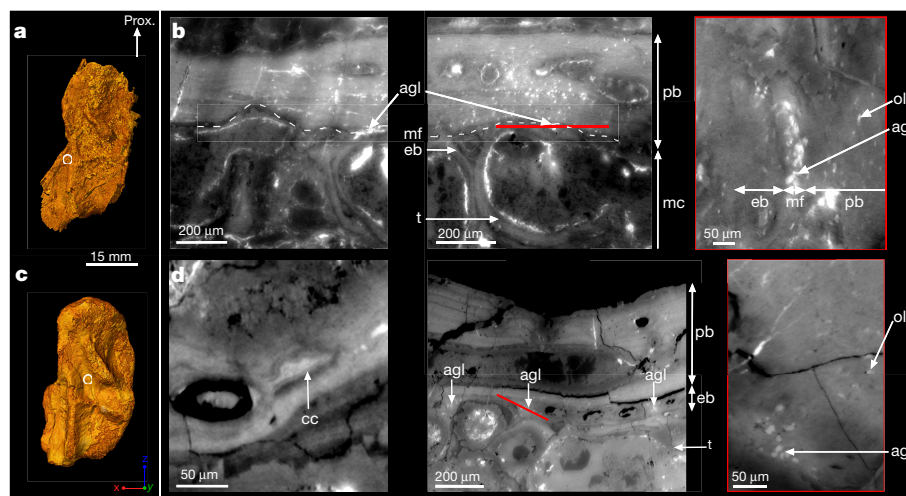
Figure 2 | Humeral bone development. a, Three-dimensional model of the humerus of NHMD 74756 in dorsal view. The white circle indicates the midshaft location of the virtual thin sections in **b. b,** Humeral cortical histology (voxel size: 0.638 μm; thickness: 10 μm) showing the complete bone deposit of periosteal bone (pb) from the mineralization front (mf) to the surface of the humerus. The aligned globular cell lacunae (agl) are identified as remnants of chondrocyte lacunae, which are much larger than osteocyte lacunae (ol), and typically closely aligned in rows. Trabeculae (t) are numerous in the medullary cavity (mc) and covered with endosteal bone (eb). From left to right: longitudinal virtual thin section; transverse virtual thin section showing the location of the next section in red; tangential virtual thin section. **c,** Three-dimensional model of the humerus of MGUH 29020 in dorsal view showing the high-resolution scanned location. **d,** Humeral cortical histology (voxel size: 0.638 μm; thickness: 10 μm) showing the complete record of cortical bone deposition. In addition, remnants of calcified cartilage (cc) within the trabeculae explain their endochondral origin. From left to right: longitudinal virtual thin section in the trabecular region; transverse virtual thin section showing the location of the next section in red; oblique virtual thin section.

Figure 3 | Bone skeletochronology. a, Three-dimensional models of the humeri of MGUH 29020 (left) and NHMD 74756 (right) in dorsal and ventral views, showing the locations of the high-resolution scans. **b–e,** Virtual thin sections revealing lines of arrested growth (yellow and white arrows) resulting from the cyclical growth of the cortical deposit (c). **b,** Longitudinal section (voxel size: 0.638 μm; thickness: 30 μm). **c,** Transverse section (voxel size: 0.638 μm; thickness: 30 μm). **d,** Transverse section (voxel size: 1.12 μm; thickness: 80 μm). **e,** Transverse section (voxel size: 0.638μm; thickness: 30μm). The annual bone growth rate (Extended Data Table 1) was measured in each specimen in regions of cortical bone not distorted by taphonomic or biological factors (such as muscle insertions) and exhibiting regular LAG patterns labelled with white arrows.

preservation of the bone itself and can potentially be matched in a wide range of stem tetrapods. Even a single limb bone can, in principle, provide decisive answers to questions about the length of the juvenile stage and the onset of limb ossification, which in turn help to constrain palaeobiological hypotheses. We are undertaking a systematic PPC-SRμCT survey of stem tetrapod limb histology with this aim in mind. For now, *Acanthostega* provides a first glimpse of the life history of a Devonian tetrapod.

Online Content Methods, along with any additional Extended Data display items and Source Data, are available in the online version of the paper; references unique to these sections appear only in the online paper.

1. Clack, J. A. *Gaining Ground* 2nd edn (Indiana Univ. Press, 2012).
2. Niedźwiedzki, G., Szrek, P., Narkiewicz, K., Narkiewicz, M. & Ahlberg, P. E. Tetrapod trackways from the early Middle Devonian period of Poland. *Nature* **463,** 43–48 (2010).
3. Shubin, N. H., Daeschler, E. B. & Jenkins, F. A., Jr. The pectoral fin of *Tiktaalik roseae* and the origin of the tetrapod limb. *Nature* **440,** 764–771 (2006).
4. Friedman, M., Coates, M. I. & Anderson, P. First discovery of a primitive coelacanth fin fills a major gap in the evolution of lobed fins and limbs. *Evol. Dev.* **9,** 329–337 (2007).
5. Boisvert, C. A., Mark-Kurik, E. & Ahlberg, P. E. The pectoral fin of *Panderichthys* and the origin of digits. *Nature* **456,** 636–638 (2008).
6. Astin, T. R., Marshall, J. E. A., Blom, H. & Berry, C. M. The sedimentary environment of the Late Devonian East Greenland tetrapods. *Geol. Soc. Lond.* **339,** 93–109 (2010).
7. Blom, H., Clack, J. A., Ahlberg, P. E. & Friedman, M. Devonian vertebrates from East Greenland: a review of faunal composition and distribution. *Geodiversitas* **29,** 119–141 (2007).
8. Sanchez, S., Ahlberg, P. E., Trinajstic, K. M., Mirone, A. & Tafforeau, P. Three-dimensional synchrotron virtual paleohistology: a new insight into the world of fossil bone microstructures. *Microsc. Microanal.* **18,** 1095–1105 (2012).
9. Warburton, F. E. & Denman, N. S. Larval competition and the origin of tetrapods. *Evolution* **15,** 566 (1961).
10. Blom, H., Clack, J. A. & Ahlberg, P. E. Localities, distribution and stratigraphical context of the Late Devonian tetrapods of East Greenland. *Medd. Gronl.* **43,** 4–50 (2005).
11. Clack, J. A. The dermal skull roof of *Acanthostega gunnari*, an early tetrapod from the Late Devonian. *Trans. R. Soc. Edinb. Earth Sci.* **93,** 17–33 (2002).
12. Callier, V., Clack, J. A. & Ahlberg, P. E. Contrasting developmental trajectories in the earliest known tetrapod forelimbs. *Science* **324,** 364–367 (2009).

13. Coates, M. I. The Devonian tetrapod *Acanthostega gunnari* Jarvik: postcranial anatomy, basal tetrapod interrelationships and patterns of skeletal evolution. *Trans. R. Soc. Edinb. Earth Sci.* **87**, 363–421 (1996).

14. Sanchez, S., Tafforeau, P. & Ahlberg, P. E. The humerus of *Eusthenopteron*: a puzzling organization presaging the establishment of tetrapod limb bone marrow. *Proc. R. Soc. Lond. B* **281**, 20140299 (2014).

15. Coates, M. I., Ruta, M. & Friedman, M. Ever since Owen: changing perspectives on the early evolution of tetrapods. *Annu. Rev. Ecol. Evol. Syst.* **39**, 571–592 (2008).

16. Francillon-Vieillot, H. *et al.* in *Skeletal Biomineralization: Patterns, Processes and Evolutionary Trends.* (ed. J. G. Carter) Vol. I., 471–530 (Van Nostrand Reinhold, 1990).

17. Laurin, M., Meunier, F.-J., Germain, D. & Lemoine, M. A microanatomical and histological study of the paired fin skeleton of the Devonian sarcopterygian *Eusthenopteron foordi. J. Paleontol.* **81**, 143–153 (2007).

18. Castanet, J., Francillon-Vieillot, H. & de Ricqlès, A. in *Amphibian Biology* (eds H. Heatwole & M. Davies) Vol. V Osteology, 1598–1683 (Surrey Beatty & Sons, 2003).

19. Padian, K. Evolutionary physiology: A bone for all seasons. *Nature* **487**, 310–311 (2012).

20. Sanchez, S., Klembara, J., Castanet, J. & Steyer, J.-S. Salamander-like development in a seymouriamorph revealed by palaeohistology. *Biol. Lett.* **4**, 411–414 (2008).

21. Castanet, J., Francillon-Vieillot, H., Meunier, F.-J. & de Ricqlès, A. in *Bone* (ed. B. K. Hall) Vol. 7: Bone Growth B, 245283 (CRC Press, 1993).

22. Fröbisch, N. B. Ossification patterns in the tetrapod limb–conservation and divergence from morphogenetic events. *Biol. Rev. Camb. Philos. Soc.* **83**, 571–600 (2008).

23. Witzmann, F. Developmental patterns and ossification sequence in the Permo-Carboniferous temnospondyl *Archegosaurus decheni* (Saar-Nahe Basin, Germany). *J. Vertebr. Paleontol.* **26**, 717 (2006).

24. Schoch, R. R. Skeleton formation in the Branchiosauridae: a case study in comparing ontogenetic trajectories. *J. Vertebr. Paleontol.* **24**, 309–319 (2004).

25. Peacor, S. D. & Pfister, C. A. Experimental and model analyses of the effects of competition on individual size variation in wood frog (*Rana sylvatica*) tadpoles. *J. Anim. Ecol.* **75**, 990–999 (2006).

26. Badyaev, A. V. Growing apart: an ontogenetic perspective on the evolution of sexual size dimorphism. *Trends Ecol. Evol.* **17**, 369–378 (2002).

27. Kind, P. K. *Movement Patterns and Habitat Use in the Queensland Lungfish* Neoceratodus forsteri (*Krefft 1870*) PhD Thesis, Univ. Queensland (2002).

28. Sparreboom, M. *Salamanders of the Old World: the Salamanders of Europe, Asia and Northern Africa* (KNNV Publishing, 2014).

29. Ahlberg, P. E. & Milner, A. R. The origin and early diversification of tetrapods. *Nature* **368**, 507–514 (1994).

30. Johanson, Z. The Upper Devonian fish *Bothriolepis* (Placodermi: Antiarchi) from near Canowindra, New South Wales, Australia. *Rec. Aust. Mus.* **50**, 315–348 (1998).

Supplementary Information is available in the online version of the paper.

Author Contributions S.S., P.E.A. and P.T. conceived and designed the project. S.S. and P.T. performed the synchrotron experiments. The localities were excavated by J.A.C. and P.E.A. in 1987. P.T. processed and reconstructed the raw PPC-SRµCT scan data. S.S. segmented the scan data. S.S., P.E.A. and P.T. analysed the data. All authors discussed the interpretations. S.S. and P.E.A. developed the main text. S.S. made the figures and supplementary information. All authors provided a critical review of the manuscript and approved the final draft.

Author Information The synchrotron data will be made available through the ESRF palaeontology database (http://paleo.esrf.eu). Reprints and permissions information is available at www.nature.com/reprints. The authors declare no competing financial interests. Readers are welcome to comment on the online version of the paper. Correspondence and requests for materials should be addressed to S.S. (sophie.sanchez@ebc.uu.se).

Reviewer Information *Nature* thanks J. Anderson, N. Fröbisch, R. Schoch and K. Stein for their contribution to the peer review of this work.

METHODS

Sampling protocol. All the humeri of *Acanthostega* known so far from the Upper Devonian locality of Stensiö Bjerg (East Greenland) were brought together from museum collections to perform the current study (Natural History Museum of Denmark: MGUH 29019, MGUH 29020, NHMD 74756, University Museum of Zoology Cambridge: UMZC T.1295). They were all imaged at both low and high resolutions at beamline ID19 of the ESRF (see experimental parameters below).

In the diaphyseal region, nine homologous regions were investigated at high resolution in the four humeri but only regions 2, 3, 7, 8 and 9 could provide quantifiable information regarding growth patterns (Extended Data Figs 4, 6 and Extended Data Table 1). Areas of muscle insertion[31] were avoided as much as possible. Most of the regions (2, 3, 9) are non-muscle attachment areas. Regions 7 and 8 are located between two regions of muscle insertions but their LAG patterns remain undisturbed (Fig. 3e and Extended Data Fig. 5a). Only the LAG pattern of region 7 of MGUH 29020 (Extended Data Fig. 5b) presents an inner cortex that is highly vascularised. In this case, measurements were done in the most external part of the cortex exhibiting a regular untouched LAG pattern.

In the epiphyseal region, one scan was performed at high resolution in specimen MGUH 29020.

Imaging experiments. X-ray imaging was done using propagation phase-contrast synchrotron microtomography (PPC-SRμCT) at beamline ID19 of the ESRF. A multiscale approach allowed us to perform scans with voxel sizes varying from 20.24 to 0.638 μm with average energies ranging from 60 to 123 keV

Low-resolution experiments. The scan of MGUH 29020, at 20.24 μm voxel size, was done with a monochromatic beam, using a double Si111 Bragg monochromator and a FReLON 2k14 CCD detector[32] mounted on the lens coupling optics. The optical system was associated to a Gadox scintillator of 20 μm thickness. The distance between the sample and detector was 950 mm. The scans were performed at 60 keV.

NHMD 74756 was imaged with a voxel size of 14.95 μm with a monochromatic beam, using a double Si111 Bragg monochromator and a 2k14 CCD detector[31]. The optical system was associated to a Gadox scintillator of 10 μm thickness. The sample was positioned 900 mm from the detector. The scans were performed at 60 keV. 5,000 projections were taken over 360° in half-acquisition mode. The time of exposure was of 0.25 s.

In order to obtain a voxel size of 12.62 μm while scanning humeri MGUH 29019, MGUH 29020 and UMZC T.1295, the experiment was done using pink beam with a Frelon 2k14 CCD detector[31] mounted on an optical system associated to a 1,000-μm-thick LuAG scintillator. The gap of the wiggler was opened to 50 mm. The beam

was filtered with 2 mm of aluminium and 9 mm of copper. The resulting average energy was of 123 keV. The samples were placed 13 m from the detector in order to obtain an enhanced propagation phase-contrast. 4,998 projections were taken over 360° in half-acquisition mode. The time of exposure was of 0.15 s.
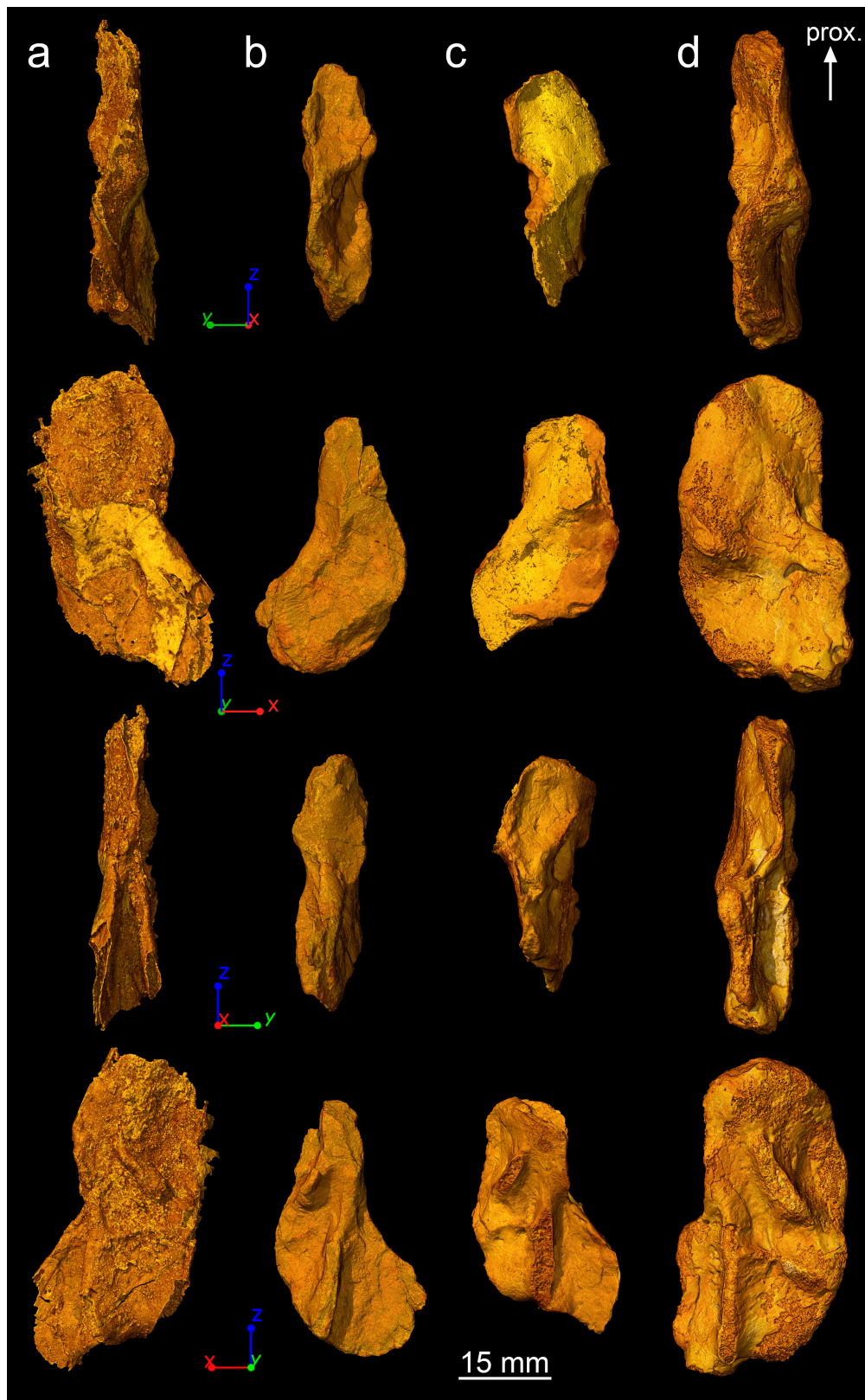
High-resolution experiments. The epiphysis of MGUH 29020 was imaged with a voxel size of 1.12 μm. The experiment was performed in monochromatic conditions with a FReLoN 2K14 (ref. 32), a 10× objective, N.A. 0.3, coupled with a 2.5× eyepiece and a 10-μm-thick GGG scintillator mounted on the microscope optics in binning conditions. The multilayer was set to the energy of 52 keV. The distance of propagation was of 150 mm.

The high-resolution scans at midshaft were done with a voxel size of 0.638 μm using pink beam. A Frelon 2k14 CCD detector[32] associated to a microscope with a 25 μm-thick GGG scintillator allowed us to obtain a sub-micrometre voxel size. The gap of the U32u undulator was 11.5 mm. The beam was filtered with 2 mm of aluminium, 0.1 mm of copper and 0.1 mm of tungsten. The average energy was probably 55 keV. Twenty-two transfocator 2D CRL lenses, made of beryllium and with a radius of curvature of 0.5 mm, were used to reduce the divergence of the beam at this energy, thereby increasing the flux going through the samples. The fossils were at a distance of propagation of 150 mm. 6,000 projections were taken over 360° in half-acquisition mode. The time of exposure was 1 s.
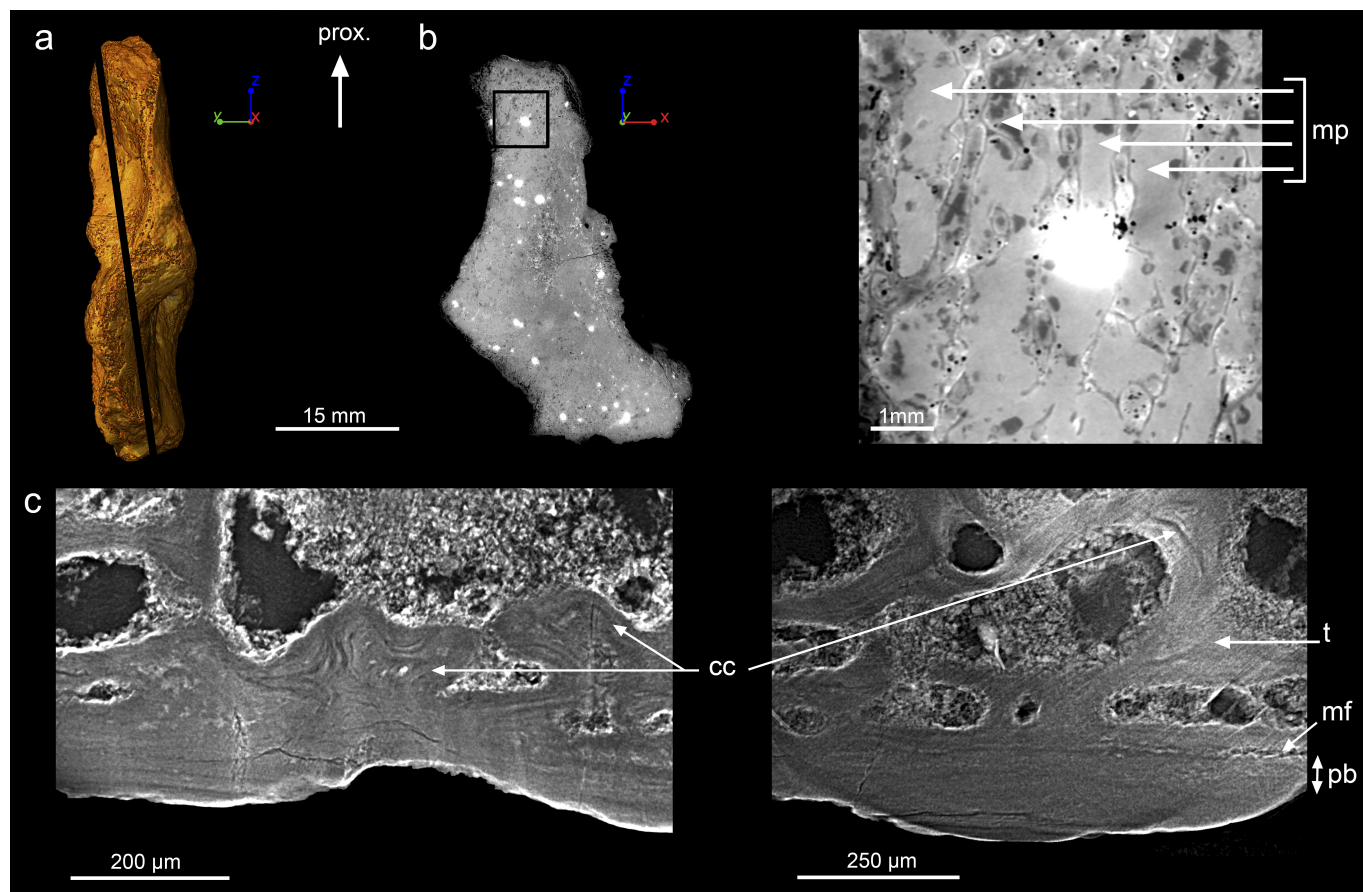
Image reconstruction. The data were reconstructed using a single distance phase retrieval approach[8] based on a modified version of the algorithm of Paganin *et al.*[33], applying an unsharp mask to the radiographs after the phase retrieval to compensate for the partial loss of high frequencies due to the original algorithm. This is based on a relative chemical homogeneity assumption. In-house filters were used to enhance the contrast between the microstructures and to reduce the noise induced by metallic infillings.

Segmentation. The data were segmented using VGStudio MAX version 2.2 software (Volume Graphics Inc.).

31. Bishop, P. J. The humerus of *Ossinodus pueri*, a stem tetrapod from the Carboniferous of Gondwana, and the early evolution of the tetrapod forelimb. *Alcheringa Australas. J. Palaeontol.* **38,** 209–238 (2014).
32. Labiche, J.-C. *et al.* Invited article: the fast readout low noise camera as a versatile x-ray detector for time resolved dispersive extended x-ray absorption fine structure and diffraction studies of dynamic problems in materials science, chemistry, and catalysis. *Rev. Sci. Instrum.* **78,** 091301–091311 (2007).
33. Paganin, D., Mayo, S. C., Gureyev, T. E., Miller, P. R. & Wilkins, S. W. Simultaneous phase and amplitude extraction from a single defocused image of a homogeneous object. *J. Microsc.* **206,** 33–40 (2002).
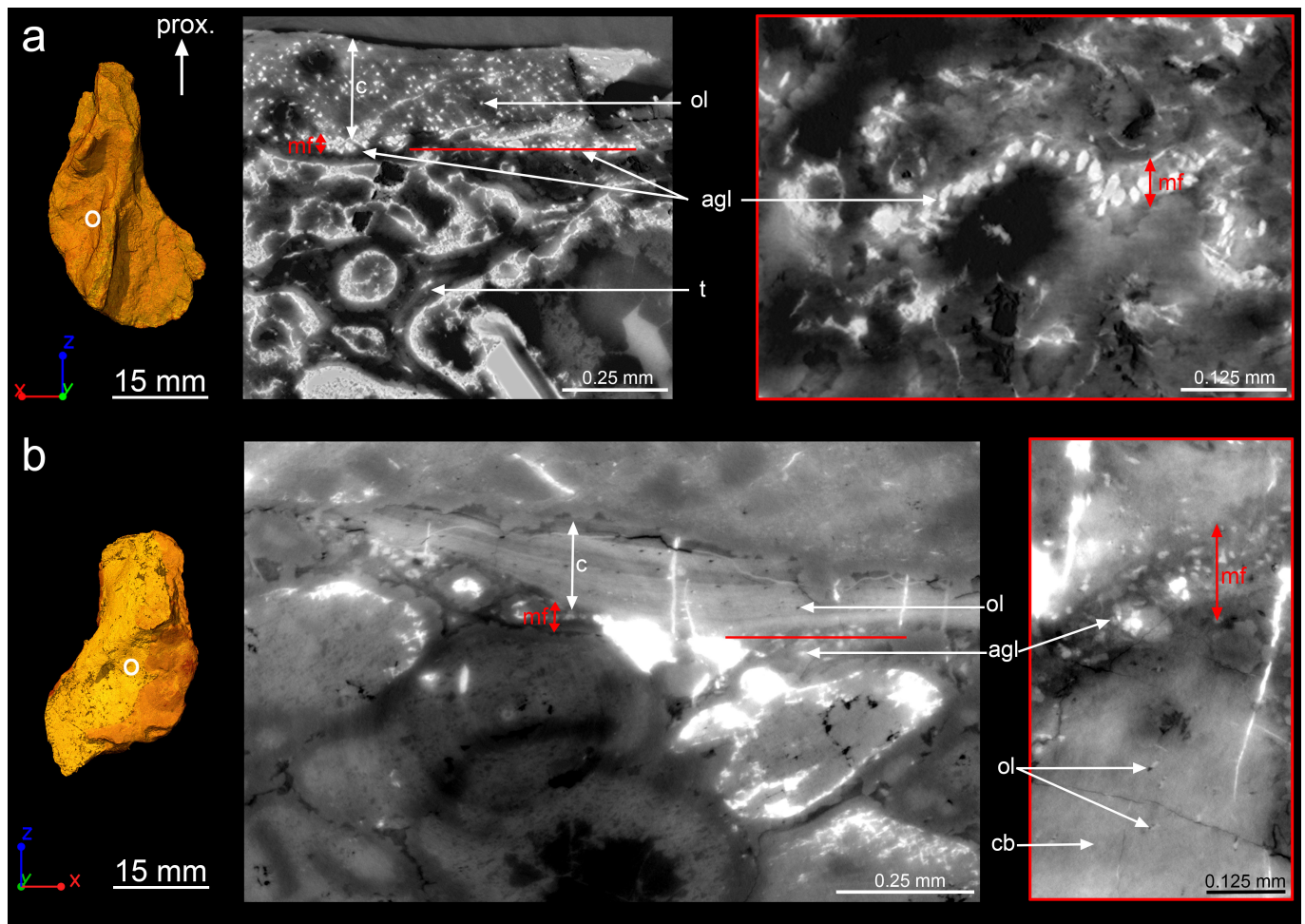
Extended Data Figure 1 | Three-dimensional models of *Acanthostega* humeri based on synchrotron microtomography data. a, NHMD 74756. **b**, UMZC T.1295. **c**, MGUH 29019. **d**, MGUH 29020. From top to bottom: preaxial view, ventral view, postaxial view, dorsal view. Humeri are all oriented with their proximal epiphysis towards the top.
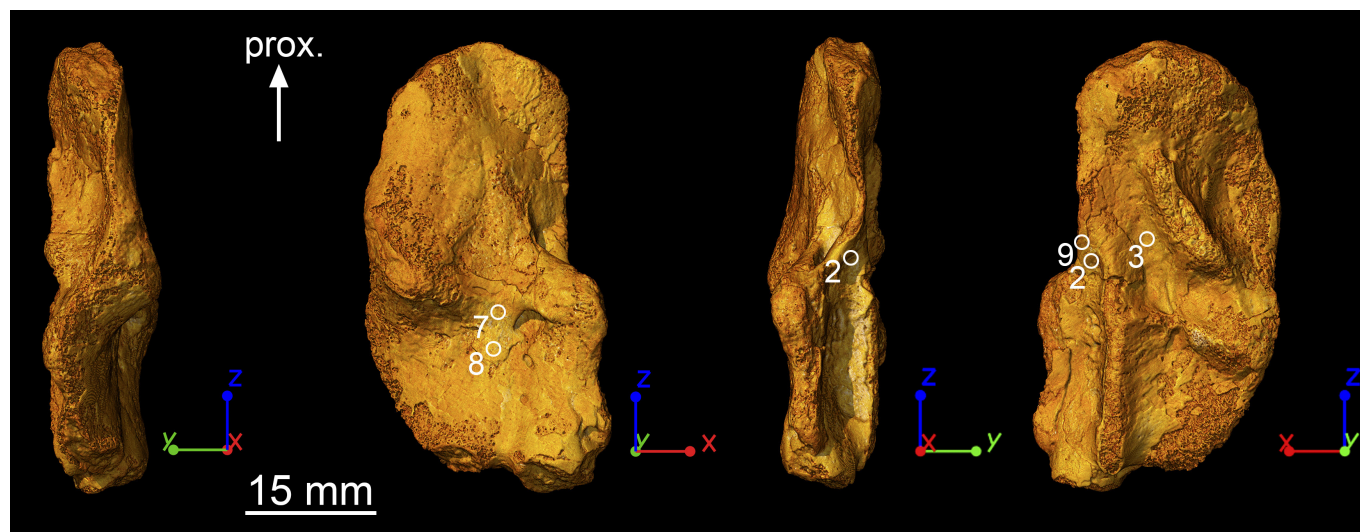
Extended Data Figure 2 | Epiphyseal microanatomy and histology of *Acanthostega* **humerus (MGUH 29020). a,** Three-dimentional model in preaxial view, based on synchrotron microtomography data, oriented with the proximal extremity (epiphysis[6]) towards the top. The black line indicates the virtual thin section illustrated in **b. b,** Longitudinal virtual thin section (thickness: 50 μm, voxel size: 1.12 μm, same scale bar and orientation as in **a**) showing the location of the detailed image on the right. The latter shows the marrow processes (mp) formed in the growth plate by endochondral ossification. **c,** High-resolution virtual thin section (thickness: 50 μm, voxel size: 1.12 μm) from the epiphyseal region showing obvious Liesegang's rings as remnants of calcified cartilage[6] (cc), formed during endochondral ossification. These remnants are entrapped in the trabeculae (t), at the vicinity of the ossification notch[6], where the thickness of the periosteal bone (pb) between the mineralization front (mf) and the surface is greatly reduced. The bone is oriented with its surface towards the bottom. Left, longitudinal thin section; right, transverse section.
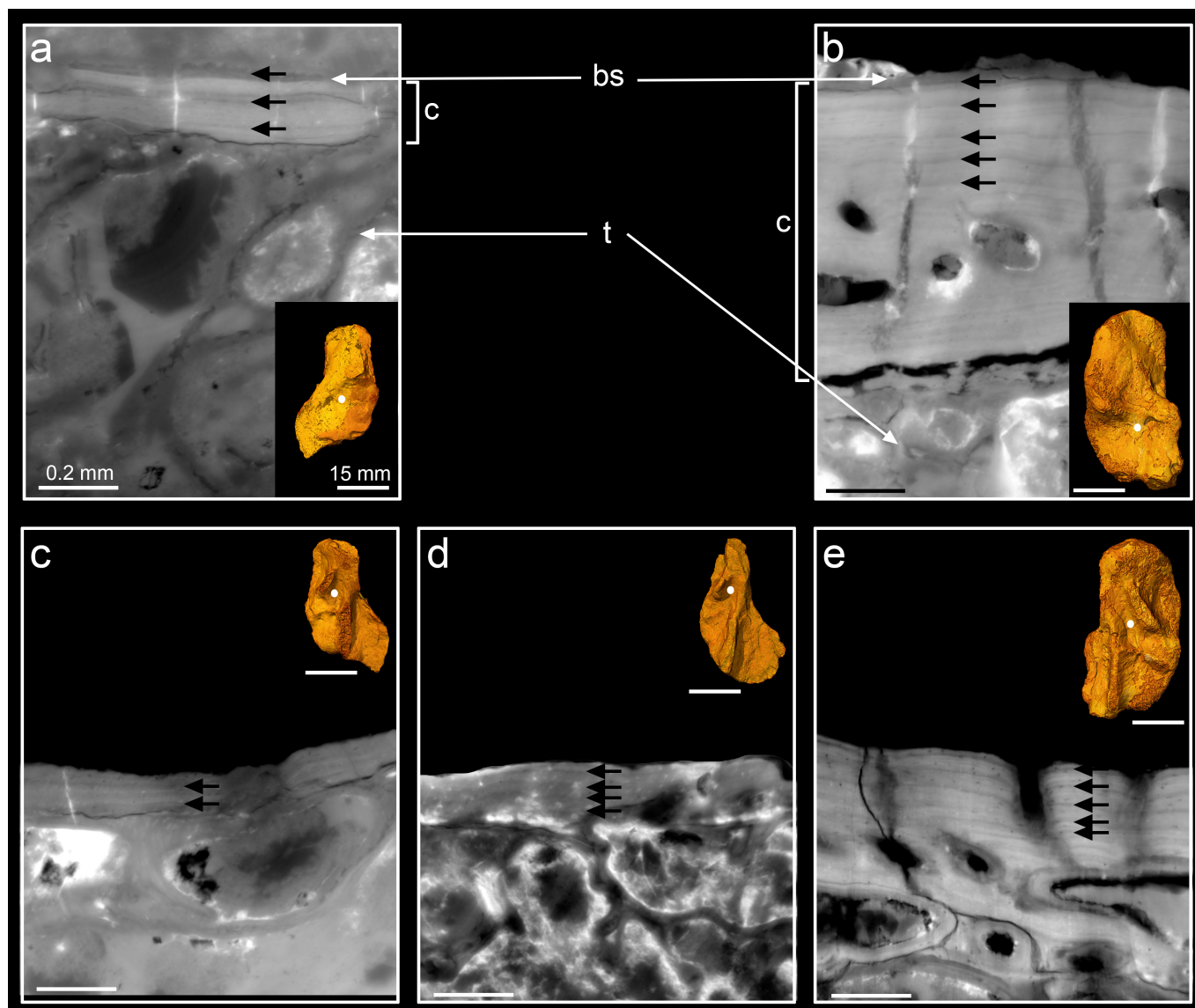
Extended Data Figure 3 | Midshaft bone histology of two *Acanthostega* humeri (UMZC T.1295 and MGUH 29019). a, Three-dimensional model of humerus UMZC T.1295 in dorsal view and oriented with the proximal epiphyses[6] towards the top. The white circle indicates the midshaft location at which the transverse virtual section was made. The latter (single tomographic slice, voxel size: 0.638 μm) shows the complete bone deposit of cortical bone (c) from the mineralization front (mf) to the surface of the humerus (top). The cortical bone comprises numerous osteocyte lacunae (ol), which are much smaller than the aligned globular cell lacunae (agl) present at the location of the mineralization front. Trabeculae (t) are numerous in the medullary cavity. The red line in the transverse virtual section indicates the location of the next tangential virtual section which details the mineralization front. **b**, Three-dimensional model of the humerus MGUH 29019 in ventral view showing the high-resolution scanned location. The virtual section shows the humeral cortical histology at the midshaft (single tomographic slice, voxel size: 0.638 μm). As in UMZC T.1295, the cortical bone matrix (cb) is very compact, pierced with small osteocyte lacunae. At this location, its surface (top), although still embedded in the rock matrix, is not well preserved. The red line in the transverse virtual section indicates the location of the next tangential virtual section detailing the cellular structure of the mineralization front.

Extended Data Figure 4 | Regions of high-resolution scans. Skeletochronological observations were done at sub-micrometre resolution in nine homologous regions of the four humeri of *Acanthostega*. Specimen MGUH 29020 is used here to illustrate the regions providing quantifiable informa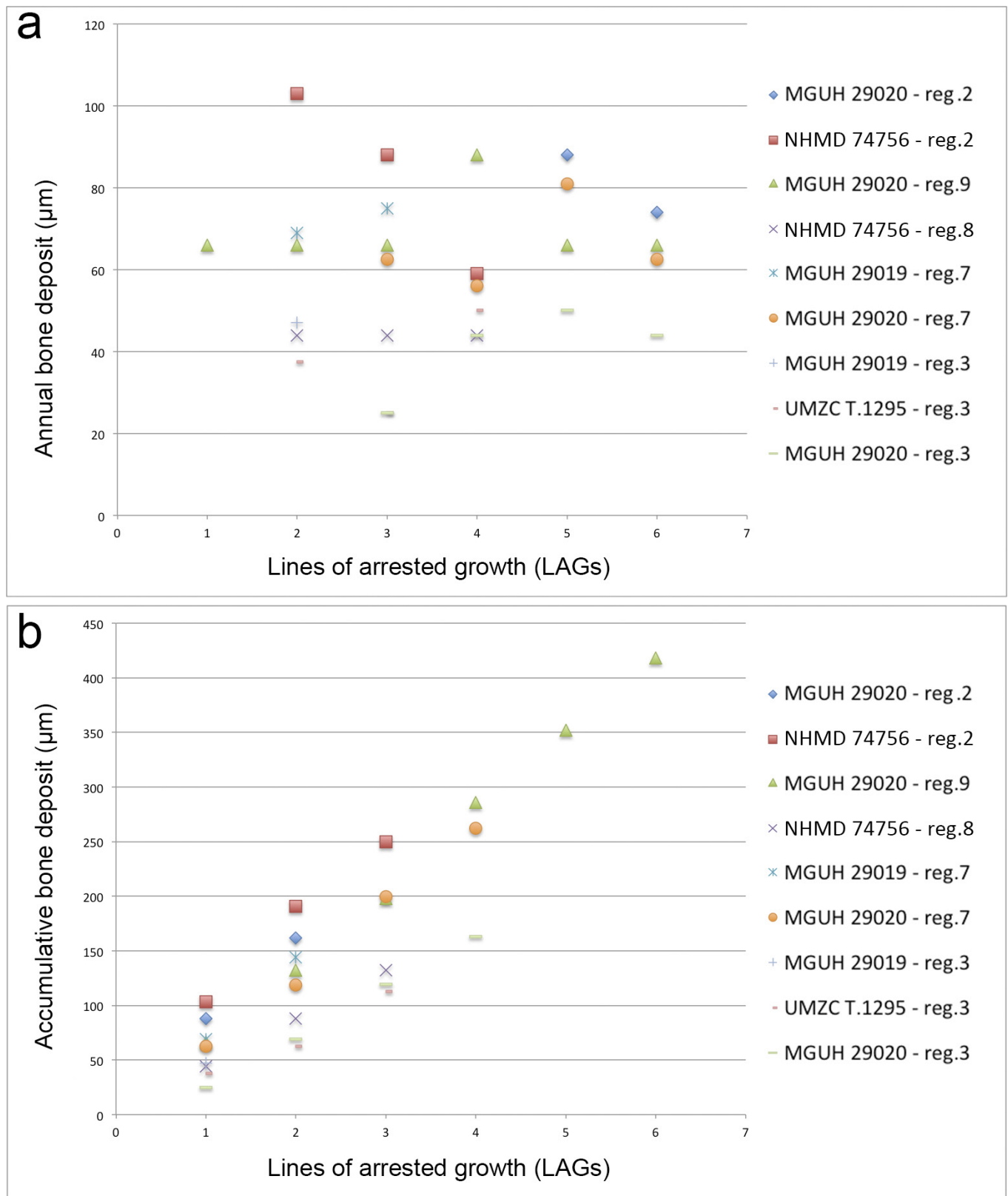tion to calculate annual bone growth rates (Extended Data Table 1). Areas of muscle insertion were avoided when possible. Regions 2, 3 and 9 are non-muscle attachment areas. Regions 7 and 8 are located between two regions of muscle insertions but annual bone growth rates (Extended Data Table 1) were measured only in undisturbed cortical parts exhibiting regular LAG patterns.

Extended Data Figure 5 | Humeral midshaft skeletochronology.
All virtual thin sections (voxel size: 0.638 μm) reveal LAGs (black arrows) resulting from the cyclical growth of the cortical deposit (c). They are oriented with the surface of the bone (sb) towards the top and medullary trabeculae (t) downwards. The locations of the thin sections are shown as white dots on the associated 3D models. All 3D models are oriented with their proximal epiphyses[6] towards the top. **a**, Transverse virtual thin section (thickness: 30 μm) showing three LAGs in the cortical bone of the ventral midshaft of the humerus MGUH 29019 (region 7). The inner surface of the cortical bone has been eroded. **b**, Longitudinal virtual thin section (thickness: 30 μm) showing five LAGs in the cortical bone of the ventral midshaft of MGUH 29020 (region 7). The inner cortical bone is disturbed by a highly vascularised period. LAGs cannot be identified with accuracy in this region. The growth deposits between the LAGs in region 7 are similar in MGUH 29019 and MGUH 29020 (Extended Data Table 1). **c**, Transverse virtual thin section (thickness: 30 μm) showing two LAGs in the cortical bone of the dorsal midshaft of the specimen MGUH 29019 (region 3). **d**, Longitudinal virtual thin section (thickness: 50 μm) showing four LAGs in the cortical bone of the dorsal midshaft of UMZC T.1295 (region 3). **e**, Longitudinal virtual thin section (thickness: 30 μm) showing five LAGs in the cortical bone of the dorsal midshaft of MGUH 29020 (region 3). The growth deposits between the LAGs in region 3 are similar in UMZC T.1295, MGUH 29019 and MGUH 29020 (Extended Data Table 1). Scale bars for virtual thin sections: 0.2 mm. Scale bars for 3D models: 15 mm.

Extended Data Figure 6 | Graphic visualizations of bone deposits.
Images are based on the measurements provided in Extended Data Table 1.
a, Amount of bone deposited every year—that is, between two LAGs—in the regions of interest (reg.) of the four studied humeri. Except for region 2 (measured in MGUH 29020 and NHMD 74756), all regions show a relatively constant or increasing growth rate during animal development. **b**, Bone deposition accumulated to form the cortex. Despite a slight variation in values due to growth allometries, the growth rate (illustrated by the slope angle) is relatively constant in all regions of all specimens, meaning that all specimens grew at the same rate.

Extended Data Table 1 | Measurements of humeral cyclical growth deposits between LAGs

Region	Specimen	Figure	LAG 0-1	LAG 1-2	LAG 2-3	LAG 3-4	LAG 4-5	LAG 5-6	Average deposit
2	MGUH 29020	Fig. 3b	LAG pattern disturbed in a highly vascularised region				88	74	81
2	NHMD 74756	Fig. 3c	eroded	103	88	59	-	-	83
9	MGUH 29020	Fig. 3d	66	66	66	88	66	66	70
8	NHMD 74756	Fig. 3e	eroded	44	44	44	-	-	44
7	MGUH 29019	Extended Data Fig. 5a	eroded	69	75	-	-	-	72
7	MGUH 29020	Extended Data Fig. 5b	LAG pattern disturbed in a highly vascularised region		62.5	56	81	62.5	65.5
3	MGUH 29019	Extended Data Fig. 5c	eroded	47	-	-	-	-	47
3	UMZC T.1295	Extended Data Fig. 5d	eroded	37.5	25	50	-	-	37.5
3	MGUH 29020	Extended Data Fig. 5e	LAG pattern disturbed in a highly vascularised region		25	44	50	44	41

Measurements (in μm) are based on the LAGs labelled with white arrows in Fig. 3 and black arrows in Extended Data Fig. 5. Nine regions were investigated but only regions 2, 3, 7, 8 and 9 could provide quantifiable information (Extended Data Fig. 4). A dash indicates that there were no more LAGs as the bone had stopped growing.